Taylor & Francis
Taylor & Francis Group

Just Accepted by *Nanotoxicology*

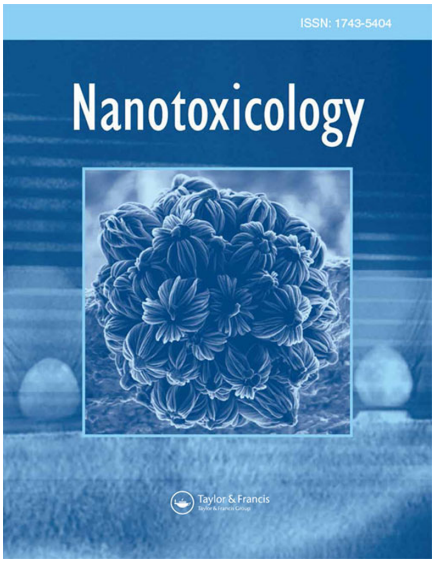

Integrative Functional Transcriptomic Analyses Implicate Specific Molecular Pathways in pulmonary toxicity from Exposure to Aluminum Oxide Nanoparticles

Xiaobo Li, Chengcheng Zhang, Qian Bian, Na Gao, Xin Zhang, Qingtao Meng, Shenshen Wu, Shizhi Wang, Yankai Xia, Rui Chen

Doi: 10.3109/17435390.2016.1149632

Abstract

Gene expression profiling has developed rapidly in recent years and it can predict and define mechanisms underlying chemical toxicity. Here, RNA microarray and computational technology were used to show that aluminum oxide nanoparticles (Al_2O_3 NPs) were capable of triggering up-regulation of genes related to the cell cycle and cell death in a human A549 lung adenocarcinoma cell line. Gene expression levels were validated in Al_2O_3 NPs exposed A549 cells and mice lung tissues, most of which showed consistent trends in regulation. Gene-transcription factor network analysis coupled with cell- and animal-based assays demonstrated that the genes encoding *PTPN6, RTN4, BAX* and *IER* play a role in the biological responses induced by the nanoparticle exposure, which caused cell death and cell cycle arrest in the G2/S phase. Further, down-regulated *PTPN6* expression demonstrated a core role in the network, thus expression level of *PTPN6* was rescued by plasmid transfection, which showed ameliorative effects of A549 cells against cell death and cell cycle arrest. These results demonstrate the feasibility of using gene expression profiling to predict cellular responses induced by nanomaterials, which could be used to develop a comprehensive knowledge of nanotoxicity.

Integrative Functional Transcriptomic Analyses Implicate Specific Molecular Pathways in pulmonary toxicity from Exposure to Aluminum Oxide Nanoparticles

Xiaobo Li[a], Chengcheng Zhang[a], Qian Bian[b], Na Gao[c], Xin Zhang[a], Qingtao Meng[a], Shenshen Wu[a], Shizhi Wang[a] , Yankai Xia [d,#], Rui Chen[a, e,#,*]

[a] Key Laboratory of Environmental Medicine Engineering, Ministry of Education, School of Public Health, Southeast University, Nanjing 210009, China

[b] Department of Toxicology and Function Assessment, Jiangsu Provincial Center for Disease Prevention and Control, Nanjing 210009, China

[c] Institute of Bioinformatics, Heinrich Heine University, Dusseldorf 40225, Germany

[d] Key Laboratory of Modern Toxicology of Ministry of Education, School of Public Health, Nanjing Medical University, Nanjing 211166, China

[e] State Key Laboratory of Bioelectronics, Southeast University, Nanjing 210096, China

[#] These authors contribute equally to this work

[*] Correspondence should be addressed to

Rui Chen

Key Laboratory of Environmental Medicine Engineering, Ministry of Education

School of Public Health, Southeast University

Dingjiaqiao 87, Nanjing, 210009, China

Email: 101011816@seu.edu.cn

Tel: 0086-25-83272560

Fax: 0086-25-83272583

Key words: aluminum oxide nanoparticle; microarray; cell cycle; cell death, nanotoxicology

ABSTRACT

Gene expression profiling has developed rapidly in recent years and it can predict and define mechanisms underlying chemical toxicity. Here, RNA microarray and computational technology were used to show that aluminum oxide nanoparticles (Al_2O_3 NPs) were capable of triggering up-regulation of genes related to the cell cycle and cell death in a human A549 lung adenocarcinoma cell line. Gene expression levels were validated in Al_2O_3 NPs exposed A549 cells and mice lung tissues, most of which showed consistent trends in regulation. Gene-transcription factor network analysis coupled with cell- and animal-based assays demonstrated that the genes encoding *PTPN6, RTN4, BAX* and *IER* play a role in the biological responses induced by the nanoparticle exposure, which caused cell death and cell cycle arrest in the G2/S phase. Further, down-regulated *PTPN6* expression demonstrated a core role in the network, thus expression level of *PTPN6* was rescued by plasmid transfection, which showed ameliorative effects of A549 cells against cell death and cell cycle arrest. These results demonstrate the feasibility of using gene expression profiling to predict cellular responses induced by nanomaterials, which could be used to develop a comprehensive knowledge of nanotoxicity.

Introduction

Because of the increased number of applications of nanoparticles available today, protecting the human respiratory system from exposure to these manufactured ultrafine particulates has become a considerable health concern. Nanomaterials differ from their corresponding conventional materials not only in scale but also in their physical, chemical, and biological characteristics. Generally, nano-scale materials are more likely to be toxic than the same materials of conventional size and can be inhaled more deeply into the lungs .For this reason, the respiratory tract is considered the primary target organ for inhaled nanoparticles. Moreover, the common mechanisms of clearance are often ineffective (Oberdorster et al., 2005), so inhaled nanosized materials can either remain within the respiratory system, which imply long-term contact between nanoparticles and alveoli, or become translocated to other target organs. A549 cell line was first initiated from an explanted lung carcinoma. It is widely used as a model of type II alveolar epithelium, representing cells from the alveoli (Ingvarsson et al., 2014, Feliu et al., 2015);(Mascelloni et al., 2015). In the present study, A549 cells and mice were used to assess the potential respiratory toxicity of inhaled Al_2O_3 nanoparticles.

Aluminum oxide (Al_2O_3) nanoparticles (NPs) are widely studied and used in chemical, industrial, and medical fields(Popat et al., 2004, Cho et al., 2006) . Further, aluminum (AL) is one of the most common heavy metal components of airborne ultrafine particles (PM2.5) in an ambient environment (Veranth et al., 2007, Reff et al., 2009). They are associated with various adverse biological effects (Bell et al., 2010, Ebisu and Bell, 2012). Aluminum in the environment is relatively stable in the form of aluminum oxide and these ultrafine particles

can enter the body through inhalation. In this way, both environmental and occupational exposure to Al_2O_3 NPs are likely increasing and may represent a serious health risk.

The toxicity of Al_2O_3 NPs has been evaluated in a wide range of studies, which have focused on lung tissue (Wagner et al., 2007, Simon-Deckers et al., 2008), the central nervous system (Li et al., 2009), liver (Hussain et al., 2005), and other vital organs(Di Virgilio et al., 2010) . Because the respiratory tract is considered to be the primary target organ for inhaled nanoparticles, the toxic effects of Al_2O_3 NPs on lung tissue and the mechanisms underlying these effects have been investigated thoroughly. For *in vivo* studies, aluminum oxide-based nano whiskers were found to promote increases in the number of lung macrophages in mice (Adamcakova-Dodd et al., 2012). Wagner et al. showed a marginal increase in rat alveolar macrophage viability induced with 24 h continuous exposure to 100 μg/mL Al_2O_3 NPs (Wagner, Bleckmann et al., 2007). Also, 53 $\mu g/cm^2$ Al_2O_3NP has been found to induce significant increases in the IL-6 response in human lung epithelial cells BEAS-2B and normal human bronchial epithelial cells in vitro (Veranth, Kaser et al., 2007). Al_2O_3 NPs can enter A549 cells rapidly and travel into the cytoplasm and intracellular vesicles (Simon-Deckers, Gouget et al., 2008). All these studies suggest a possible toxic mechanism involving inflammation, oxidative stress, and cell death.

So far, the methods used to study the effects of Al_2O_3 NPs have been mostly based on traditional in vitro assays, which only permit analyses focused on specific biological processes and well-defined molecular pathways. Large-scale “omic” approaches can often show the effects of biological pathways and processes that had not previously been known

(Cui and Paules, 2010). This makes them suitable for predicting toxicity and determining the mechanisms underlying changes induced by uncharacterized compounds(Blomme et al., 2009) . Currently, the use of "omic" techniques in toxicology studies is paving the way to new fields such as predictive toxicology (Boverhof and Zacharewski, 2006). The use of gene expression profiling is reported to study the impact of nanomaterials, including metal or metal oxide nanoparticles (Hanagata et al., 2011, Foldbjerg et al., 2012, Shim et al., 2012, Tuomela et al., 2013). However, few studies have focused on the effects of Al_2O_3 NPs on the respiratory cell lines. In our current study, modulations in gene expression profiles in A549 cells exposed to Al_2O_3 NPs were investigated using an Agilent Array platform. Results demonstrated the potential systematic cellular responses to nanomaterials.

Methods

Nanomaterials

Al_2O_3 NPs were purchased from Plasmachem GmbH, Germany (purity >99.8%). The average size and zeta potential of Al_2O_3 NPs was 64.17nm and 37.1 mV in culture medium, which was analyzed by a zetasizer (nano-zs90, Malvern Instruments, UK) (Figure S1.A and B).The morphology of Al_2O_3 NPs in PBS were determined under a transmission electron microscope (TEM) (Tecnai G2 F20, Heidelberg, Netherlands), and the particle size of Al_2O_3 NPs in PBS suspension was less than 100 nm (Figure S1B). The aggregation of Al_2O_3 NPs in PBS suspension and culture medium increased in a time-dependent manner (Figure S1C).

Cell culture and RNA extraction

According to the references, 100 μg/ml Al_2O_3 NPs treatment could trigger toxic effects in pulmonary cells(Wagner, Bleckmann et al., 2007);(Simon-Deckers, Gouget et al., 2008) , therefore, A549 cells were treated with 100 μg/ml Al_2O_3 NPs, to explore the integrative transcriptomic alterations in the present study. The human lung adenocarcinoma cell lineA549 (American Type Culture Collection) was maintained in Dulbecco's modified Eagle's medium (DMEM) at 37 °C in 5% CO_2. The culture medium was supplemented with 10% (v/v) fetal bovine serum (FBS), penicillin (100 U/ml), and streptomycin (100 μg/ml). Cells were seeded in 10 cm culture dishes and exposed to 100 μg/ml Al_2O_3 NPs with three biological replicates. Control groups were treated with culture medium. Then, 24 h after treatment, the complete medium was removed and the adherent cells were collected. Total RNA was extracted using the TRIZOL reagent (Invitrogen, US) according to the manufacturer's instructions.

RNA microarray and gene expression analysis

An Agilent Array platform (Agilent Technologies, Santa Clara, CA, US) was used for microarray analysis. mRNA was purified from total RNA after removal of rRNA using an mRNA-ONLY Eukaryotic MRNA Isolation Kit (Epicentre Biotechnologies, US). Then each mRNA sample was amplified and transcribed into fluorescent cRNA along the entire length of the transcripts without 3′ bias using a random priming method. The labeled cRNAs were hybridized onto a Human LncRNA Array v3.0 (8 × 60 K; Arraystar) chip, which is designed for 26 109 coding genes. The arrays were scanned using an Agilent G2505C scanner and the density of fluorescence was analyzed using Agilent Feature Extraction software (version

11.0.1.1). Quantile normalization and subsequent data processing were performed using the GeneSpringGx v12.0 software package (Agilent Technologies). An absolute fold change of 1.5 or more and $P = 0.05$ were set as thresholds to evaluate the significance of gene expression differences of raw data.

Functional group analysis

The DAVID 6.7 (Database for Annotation, Visualization and Integrated Discovery) functional annotation tool was used to analyze differentially expressed genes. The DAVID functional annotation cluster tool provides three structured networks of defined terms that describe the attributes of gene products. The *P*-value was set to 0.1 to denote the significance of gene ontology (GO) Term enrichment in the differentially expressed mRNA list. Then fold enrichment ((Count/Pop.Hits)/(List.Total/Pop.Total)) was set as five to denote the enrichment of a particular GO term in the input gene list compared with the population (the Homo sapiens genome).

Cell viability

Cellular viability was evaluated using a CCK-8 proliferation assay kit (Nanjing Jiancheng Bioengineering Institute, China). A549 cells were plated at a density of 1×10^4 per well in a 96-well plate and treated with 0, 12.5, 25, 50, 100, 250, 500, 1 000 μg/ml Al_2O_3 NPs with eight biological replicates for each concentration. Then 10 μL CCK-8 was added to each well and the cells were incubated for 4 h at 37°C and the absorbance was determined at 450 nm. Cell viability affected by Al_2O_3 NPs was monitored every 24 h up to seven days.

Transmission electron microscopic observation

A549 cells were treated with 100 or 500 μg/ml Al_2O_3 NPs for 24 h, then collected and fixed with 2.5% glutaraldehyde in 0.1 M sodium dihydrogen phosphate (pH 7.4). The samples were then fixed in 1% OsO_4 for 1 h, dehydrated through a graded ethanol series and gradually infiltrated with epoxy resin. Ultra-thin sections were obtained on copper grids, stained with uranyl acetate and lead citrate and observed in a transmission electron microscope (JEOL-1010, Japan).

Cell cycle analysis

A549 cells were seeded in 6-well plates at a density of about 1×10^6 cells per well, and exposed to 100 or 500 μg/ml A Al_2O_3 NPs or control medium for 24 h. All experiments were performed in sextuplicate. The cells were washed with PBS and harvested with trypsin. The cells were fixed in 75% ethanol for 24 h and then stained with propidium iodide (PI) and analyzed with a FACS Calibur Flow Cytometry (BD Biosciences, USA) to quantify the cell cycle.

Cell apoptosis analysis

Al_2O_3 NPs induced cell apoptosis were analyzed by flow cytometry with a KeyGENAnnexin V-FITC Apoptosis Detection Kit (KeyGEN BioTECH, China) according to the manufacturer's instruction. Briefly, after exposure to 100 or 500 μg/ml Al_2O_3 NPs for 24 h, A549 cells were harvested through trypsinization and washed twice with PBS. This was followed by centrifugation at 1 000 rpm for 5 min, the pellet was resuspended in 500 μl

binding buffer and incubated with 5 µl FITC-conjugated annexin V and 5 µl PI for 15 min at room temperature in the dark. The samples were analyzed by FACS Calibur Flow Cytometry (BD Biosciences, USA).

Animal treatments

Eighteen male and eighteen female ICR mice (20-22 g), were purchased from Shanghai SLRC Laboratory Animal Co., Ltd., China. Animals were treated humanely and maintained and used in accordance with Guidelines of Committee on Animal Use and Care of Southeast University. The dynamic inhalation exposure chambers were outfitted with extensive air quality monitoring equipment and an aerosol generator (Beijing HuiRongHe Technology Co., Ltd, China). Mice were divided into three groups (six female and six male mice each), here called the control, low, and high Al_2O_3 NPs treatment groups. Mice were housed six per polycarbonate cage on corncob bedding with *ad libitum* access to food and water. Exposure was carried out in three stainless-steel Hinners-type whole-body inhalation chambers; two groups received Al_2O_3 NPs, and the other received HEPA-filtered clean air at the same flow rate as the experimental group. Six male and six female mice were exposed to each chamber for 8 h per day for seven consecutive days. Light cycles were set on a 12/12 h light/dark cycle. The mean concentrations of Al_2O_3 NPs were 2 mg/m^3 and 10 mg/m^3 for low and high treatments, respectively. The temperature in the chambers was set to 22.5 °C.

Aluminum burden

Mice were euthanized under ether anesthesia 1 h after the end of dynamic Al_2O_3 NPs exposure on the 7th day. All the mice were decapitated on an iced table. Lung, heart, liver, spleen and kidney tissue samples were collected and stored in liquid nitrogen.

Approximately 0.1 g of each tissue sample was digested with HNO_3 in a boiling water bath for 3 h. The aluminum burdens in different tissues were quantified using an inductively coupled plasma mass spectrometry (ICP-MS, Agilent 7700, USA).

RNA isolation and quantitative real-time PCR assay

A549 cells were seeded in 6-well plates at a density of about 1×10^6 cells per well and exposed to 50, 100 , 250, or 500 μg/ml Al_2O_3 NPs or control medium for 24 h, then cells were trypsinized and collected. For animal tissues, a piece of left lung tissues were prepared for qRT-PCR assay.

Total RNA of A549 cells and lung tissues was extracted using the GenEluteTM Mammalian Total RNA Miniprep Kit (Sigma, US) according to the manufacturer's protocol, and the concentration of total RNA was determined by measuring the absorbance at 260 nm using a Nanodrop 2000c spectrophotometer (Thermo Scientific, US). cDNA synthesis for coding genes was performed with 1 μg of total RNA according to the manufacturer's instruction (Toyobo, Tokyo, Japan).

The mRNA levels for modulated genes were determined by reverse transcription of total RNA followed by quantitative real-time PCR analysis (qRT-PCR) on a Quant Studio 6 Flex system (Applied Biosystems, Life Technologies, US) using SYBR PCR Master Mix reagent kits (Toyobo) in accordance with the manufacturer's protocol. Primers were designed for the modulated genes screened by RNA microarray. Primer sequences are shown in Table S1and S2. All experiments were performed in triplicate. The mRNA levels given here are relative to cyclophilin A for the indicated gene.

Gene-transcription factor network analysis

The gene-transcription factor network was analyzed based on the transcriptional factor target set in the Encyclopedia of DNA Elements (ENCODE) (Gerstein et al., 2012). The dataset was downloaded from file "enets2.Proximal_filtered.xls" in the supplementary material of the paper. The figure was drawn using a free online tool cytoscape.

siRNA knockdown, plasmids construction, transfections and immunodetection

For siRNA knockdown, we transfected A549 cells in a 6-well plate with siRNAs (Thermo Fisher Scientific, USA) directed against control or *PTPN6* using DharmaFECT1 (Thermo Fisher Scientific, USA). The final concentration of *PTPN6* siRNA were 10, 20 and 40 nM, respectively. Wild-type (WT) human PTPN6 cDNA with 3' Myc epitope tagged CMV promoter-driven pCMV6-Entry expression vectors was purchased from Origene (OriGene Technologies, Beijing) as well as the pCMV6-Entry basic vector. Expression plasmids (100 ng/well) were used in transient transfection analyses. A549 cells were transfected using Lipofectamine 2000 (Invitrogen, US) in 6-well plates with a maximum of 500 ng total DNA per well. At 48 h post-transfection, cells were treated with 100 or 500 μg/ml Al_2O_3 NPs for another 24 h and then harvested.

Proteins were analyzed by immunoblotting with primary antibodies for the following antigens: human PTPN6 (1:500 dilution; Abcam, US), α-tubulin (1:10 000 dilution; Sigma, US) or c-Myc (1:5 000 dilution; Santa Cruz Biotechnology, US).

Data analysis

Values of cell viability and cell cycle assay are here expressed as means ± standard error of the mean (SEM). Statistically significant differences were determined using one-way ANOVA, followed by Dunnett's multiple comparison test. The $2^{-\Delta\Delta Ct}$ method was used to analyze the results of qRT-PCR in all experiments. Statistical analysis was performed by SPSS12.0 and the significance was set at $P < 0.05$.

Results

Overview of mRNA microarray profiles

A total of 571 mRNAs were found to be differentially expressed between the control and Al_2O_3 NPs treated A549 cells, including 464 up-regulated and 107 down-regulated genes, which were under a screening criteria with a fold change of 1.5 and $P < 0.05$ (non-adjusted) (Figure S2. A). The heatmap showed the induced and suppressed mRNA of samples exposed to Al_2O_3 relative to matched controls, which illustrates the agreement of results from volcano figure in terms of the fold-change values as 1.5, $P = 0.05$ (Figure S2.B).

To identify relevant mRNA regulated in response to Al_2O_3 NPs exposure, a more restrictive set of criteria was used for further data analysis. As shown in Table S3, the expression of 11 gene symbols were found to be increased or decreased by at least two fold change as well as an adjusted *P*-value less than 0.05 in the Al_2O_3 NPs treated samples.

GO enrichment analysis reveal regulated categories of genes

GO enrichment analysis was performed in order to better understand the mRNA changes observed in cells exposed to Al_2O_3 NPs. Significantly regulated mRNAs included 302 genes involved in biological processes (Figure 1A), 183 genes involved in molecular functions (Figure S3. A), and 228 genes involved in cellular components (Figure S3. B).

Notably, the GO category for "cell cycle" encompassing 41/302 genes (Table S4) and "cell death" encompassing 35/302 genes (Table S4), were the most strongly regulated categories.

Network analysis of key genes involved in cell cycle and cell death

The modulated genes involved in cell cycle and cell death were analyzed to show the network between genes and transcription factors. Figure 1B. shows that *APP, BRCA1, NEK5, BAX* and *PDCD4* are involved in cell cycle and cell death progress simultaneously. Further, cell death related genes *PTPN6, IER3, RTN4*, and cell cycle related gene *ID2* play central roles in this regulatory network (Figure 1B.).

Validation of mRNA expression by cell- and animal-based assays

To validate our RNA microarray data, we performed qRT-PCR to validate 11 modulated genes shown in Table S3. The A549 cell based assay showed upreguation of *CPNE7, ATP6UOD2*, N*EMF, CD44, SQSTM1, HSPA6, ZBTB7C, SLTM*, and *SRPK2* and downregulation of RPL37 and CCDC68 induced by dose-dependent Al_2O_3 NPs (Figure 2A). In mouse lung tissues, all the mRNA except that of HSPA6, which is not expressed in mice, showed the same trend in regulation with cell-based assay (Figure 2B). When compared to our array data, the expression level of *CCDC68* mRNA was lower in A549 cells and mouse

lung tissues after exposure to Al_2O_3 NPs, and the array results suggested increased regulation. The trend in regulation of other 10 mRNA was consistent with the array data (Figure 2C).

The levels of expression of thirty genes involved in cell cycle (Table S5) and thirty involved in the cell death (Table S6) were confirmed in cell- and animal-based assays. These genes arise at least twice in all the cell death or cell cycle related GO categories. Both the results of A549 cells and ICR mice lung tissues exposed to Al_2O_3 NPs showed 22/30 genes related to cell cycle (Figure 3A and B) and 22/30 genes related to the cell death whose modulation trends were consistent with array data (Figure 3C and D).

Distribution of Al_2O_3 NPs *in vivo* and *in vitro*

After 7 days Al_2O_3 NPs exposure, the significant enhancement of aluminum burden was observed in lung tissues of both low and high dose treated groups, as well as spleen of high treatment group, compared with corresponding tissue of control group.

The uptake of Al_2O_3 NPs was confirmed by TEM in A549 cells (Figure S4). Al_2O_3 NPs were localized in cytoplasm, but not observed in nucleus. They were located in cytoplasmic organelle, such as mitochondria (Figure S4B) , mostly in the endocytotic vesicles (Figure S4C).

Cell viability of A549 cells are inhibited by Al_2O_3 NPs exposure

Cytotoxicity of Al_2O_3 NPs was evaluated by CCK-8 assay. A549 cells were exposed to Al_2O_3 NPs at different doses (12.5-1 000 μg/ml) for 24 h each day for up to seven days. No significant signs of toxicity were observed in the 12.5 or 25 μg/ml Al_2O_3 NPs treatment

groups during these seven days. Significant cell toxicity was evident in the 25, 50, 100, 250, 500 and 1 000 μg/ml Al_2O_3 NPs groups 24 h after treatment. In the 50 μg/ml Al_2O_3 NPs group, significant toxicity was observed 48 h after the beginning of treatment (Figure 4A). Annexin V-FITC and PI double staining was performed to confirm the stages of cellular viability. Here, 100 and 500 μg/mL Al_2O_3 NPs treatment of A549 cells generated 22.69±0.39% and 70.31±0.57% necrotic cell populations, respectively, but no apoptotic cells were found in either treatment group (Figure 4B).

Al_2O_3NPs trigger cell cycle arrest in the A549 cell line

Since GO analysis of the mRNA data suggested that the genes that were affected primarily represented the cell cycle category, we therefore evaluated the cell cycle in A549 exposed to Al_2O_3 NPs. Remarkably, both 100 and 500 μg/ml dose exposure of cells to Al_2O_3 NPs for 24 h triggered cell cycle arrest. The data show that 100 μg/ml Al_2O_3 NPs exposure induce retention of the cells in G2/S phase, while 500 μg/ml Al_2O_3 NPs exposure only induce G2 phase arrest in A549 cells. (Figure 4C).

Bioinformatic analyses based on the confirmed genes

A total of forty mRNA were validated by qRT-PCR in A549 cells and mouse lung tissues were reanalyzed by GO enrichment genetic related disease prediction and gene-transcription factors association. The mitosis, especially G2 phase mitotic cell cycle are most strongly regulated GO categories involved in biological processes (Figure 5A). Predicted by the genetic associated disease model, 10/40 genes were confirmed to be involved in cancer and 7/40 genes in immune system. The other related disease classes included psychiatric

disorders and normal variation (Table S8). For all the validated genes, *PTPN6, BAX, IER3,* and *RTN4* showed strong regulatory abilities and associations with the transcription factors and other genes (Figure 5B). Further, PTPN6 is associated with three genes (*BAX, APP* and *PDCD4*) involved in both cell cycle and cell death pathway and 16 transcription factors, which is the most important gene in this network. The PTPN6 regulation network and heatmap of *PTPN6, APP, BAX* and *PDCD4* were shown in Figure 5C.

PTPN6 rescue demonstrates protective effects of A549 cells from cell death and cell cycle arrest

Results showed that even 10 nM *PTPN6* siRNA transfection could induce significant cell cycle arrest in S phase and loss in G1 stage in A549 cells (Figure S5). PTPN6 expression levels in Al_2O_3 NPs treated A549 cells are restored after plasmid transfection (Figure 6A) . This rescued *PTPN6* expression completely or partially prevents A549 cells from cell death and G2/S phase cell cycle arrest after exposure to 100 or 500 μg/ml Al_2O_3 NPs (Figure 6B and C).

Discussion

Using high-throughput mRNA sequencing and computational approaches, it was here shown that Al_2O_3 NPs cause changes in gene expression in A549 cells, which is the model cell to mimic the human type II alveolar epithelial cell. The levels of expression of significantly regulated genes, which are predicted by gene expression profiling, were confirmed by RT-PCR. Among the modulated genes, gene categories related to cell cycle and cell death

were among the most significantly affected categories. Further functional assays confirmed that the Al_2O_3 NPs caused cell cycle arrest and cell death but not apoptosis in A549 cells.

So far, the global analysis of changes in the expression level of genes, followed by confirmation in the cell- and animal-based assays, has provided an integrative approach to understanding of the alteration of gene categories in exposed cells (Wang et al., 2009). To date, several studies have used this approach to the examination of cells exposed to nanomaterials. In a recent study, Feliu et al. used whole transcriptome sequencing to gain insight into the cellular responses to cationic dendrimers and results showed that the cell-cycle related genes were down-regulated, which is mediated via NF-κB (Feliu, Kohonen et al., 2015). The current mRNA profile also suggests the regulation of cell cycle G2-phase related genes and was confirmed by cellular functional assays. In another recent study, Nymark et al. used microarray approaches to evaluate the effects of exposure to multi-walled carbon nanotubes in human lung cells BEAS 2B, and 26 genes with known mitochondrial functions were identified (Nymark et al., 2015). Eom et al. integrated mRNA and microRNA profiling to compare the effects of Ag nanoparticles and Ag ions on Jurkat T cells (Eom et al., 2014). They found more modulated genes in cells exposed to Ag nanoparticles than to Ag ions, especially genes in the metallothionein (MT) family. These proteins are typical biomarkers of metal exposure. These studies demonstrate that transcriptomic profiling provides an overview of the molecular mechanisms underlying nanomaterial toxicity.

In the present study, significantly modulated genes were screened using 2-fold change and an adjusted $P = 0.05$ cut-off. They were validated using real time RT-PCR by both A549 cell

and mouse exposure assays. The results of cell- and animal-based functional assay showed the same trend in regulation. Among the 11 modulated genes, trends of regulation of 10 genes were consistent with the mRNA array profiling data and this suggests the reliability of the array data. Further, the level of expression of genes related to the cell cycle and cell death were validated using cell- and animal-based assays. Over 70% of the expression of genes related to the cell cycle and cell death were confirmed by cell- and animal-based assays. These 55 genes were indicated by a cutoff of 1.5 fold change, which rendered the array data less consistent than the 11 genes screened with 2 or more fold change and adjusted $P = 0.05$. However, the gene expression levels and trends in A549 cells and mouse tissues exposed to Al_2O_3 NPs showed great consistency, which suggested the importance of confirming the array data using biological assays.

The toxicity of Al_2O_3 NPs was investigated by several research groups, and the major toxic effect was found to be oxidative stress. Al_2O_3 NPs induce oxidative stress in human mesenchymal stem cells (Alshatwi et al., 2013) and fish cell lines (CHSE-214) (Srikanth et al., 2015). In in vivo experiments, these nanomaterials induced enhanced reactive oxygen species (ROS) and altered antioxidant enzymes (Shrivastava et al., 2014). Nano-scale Al_2O_3 induced significant oxidative stress in a dose-dependent manner in rats that was not observed in rats exposed to bulk Al_2O_3 (Prabhakar et al., 2012). When analyzed through mRNA profiling and computational approaches, cell cycle and cell death were among the most significantly affected gene categories in A549 cells exposed to Al_2O_3 NPs in the present study.

Annexin V-FITC and PI staining were used to distinguish the cells with early and late apoptosis from the necrotic cells (W. Zhang et al., 2010). Apoptosis and/or cell cycle arrest of A549 cells could be induced using different metal or metal oxide nanoparticles, like sliver (Gurunathan et al., 2015), cerium oxide (CeO_2) (Mittal and Pandey, 2014), nickel oxide (NiO), and zinc oxide (ZnO) (Lai et al., 2015, Lu et al., 2015). However, the cellular toxic responses depend on the distinct physical-chemical characteristics of the nanoparticles. In the results presented here, Al_2O_3 NPs were found to have obvious necrotic effects but no obvious apoptotic effects in A549 cells. This is consistent with the mRNA functional group analysis.

Network analysis based on the array data for mRNA of genes related to the cell cycle and cell death showed a complex gene-transcription-factor-gene interaction. Subsequently, this network was modulated following the results of gene expression validation. The expression of *NEK6, YARS, RUNX3, NET1,DDX11,* and *ID2* was not observed in either cell or animal assays, further, *PTPN6, BAX, IER3, RTN4, BRCA1, PDCD4,* and *APP* play a role in the regulation of cell death and cell cycle responses. Interestingly, except the typical cell cycle involved gene *PDCD4*, cell death involved genes *PTPN6, BAX* and *IER3*. Two other genes, *RTN4* and *APP*, were shown to participate in the cell death progress of A549 cells induced by Al_2O_3 NPs.

The *RTN4* gene belongs to the family of reticulon encoding genes. Reticulons may play a role in the restriction of axonal regeneration and structural plasticity in CNS (Oertle et al., 2003). The expression of RTN4 affects cell death through upregulation of basal levels of BAX, and activation of caspase-3 (Teng and Tang, 2013). Further, expression of RTN4 can inhibit the

activity of beta-secretase beta-site APP cleaving enzyme 1 (BACE1) and therefor regulate the cleavage of APP (Murayama et al., 2006). *APP* encodes a cell surface receptor and transmembrane precursor protein, which is cleaved by secretases to form a number of peptides, some of which form the protein basis of the amyloid plaques found in the brains of patients with Alzheimer's disease (Calero et al., 2015). Aluminum is a confirmed neurotoxin and is reported to be associated with the upregulation of APP expression in brain tissues (Q. L. Zhang et al., 2012, Thenmozhi et al., 2015). These two genes demonstrate a strong association with effects on the nervous system, which could distinguish the cell death effects induced by Al_2O_3 NPs from those induced by other nanomaterials.

PTPN6 was found to be down-regulated in both cell- and animal-based assays and play a core role in the network. *PTPN6* encodes a protein that is a member of the tyrosine phosphatase (PTP) family. PTPs are known to be signaling molecules that regulate a variety of cellular processes including cell growth, differentiation, and the mitotic cycle (Lopez-Ruiz et al., 2011). In tumor cells, overexpression of PTPN6 generally increases resistance to chemotherapeutic drugs (Sooman et al., 2014) or radiotherapy (Cao et al., 2013). Suppression of PTPN6 expression showed a promotion effects of cell death (Witzig et al., 2014). Our results are consistent with these reports, down-regulated *PTPN6* expression levels play a core regulatory role in Al_2O_3 NPs induced A549 cell death and cell cycle arrest, further, the protective effects of *PTPN6* rescue were proven by cell based assays. Taken together, these data suggested that maintaining normal expression level of *PTPN6* is key to ameliorate Al_2O_3 NPs induced A549 cell damages.

In the present study, blunting of the endogenous PTPN6 levels by siRNA transfection or induced by Al_2O_3 NPs exposure do not resulted in completely similar cell cycle stage arrest in A549 cells. Regulation of *PTPN6* to cell cycle largely depends on the cellular response to different stresses. Downregulation of *PTPN6* were reported to induce G1/S phage arrest in prostate cancer cells (Rodriguez-Ubreva et al., 2010) and lung cancer cells (Cao, Ding et al., 2013); G0-G1 phase arrest in in human multiple myeloma cells. (Lee et al., 2014) and nasopharyngeal carcinoma cells (Sun et al., 2015). Khalil et al reported that during the proliferation of germinal centers generated memory B cells, expression of *SHP-1/PTPN6* was downregulated as well as dissociation of *BCR* and *SHP-1* occurred only in G2 phage, when compared with G1 and S stages. The amount of *SHP-1/PTPN6* then returned to normal level at M phase, which suggested that decreased *SHP-1/PTPN6* expression was involved in G2 stages (Khalil et al., 2012). On the other hand, overexpression of *SHP-1* were reported to induce S phase arrest (Dong et al., 1999), G0-G1 arrest (Pathak et al., 2007) in myeloid cell.

In the present study, it is exogenous chemical exposure resulted in S/G2 arrest of A549 cells. A bench of genes were modulated following Al_2O_3 exposure. The interaction and network between genes are more complicated than knockdown of one single gene with siRNA. At this point, the alterations of cell cycle arrest could be different from *PTPN6* knockdown.

Our results showed that *PTPN6* overexpression could completely or partially rescue cell cycle arrest induced by 100 or 500 μg/ml Al_2O_3 NPs (Figure 6C). These results, coupled with the bioinformatics analysis, suggested that PTPN6 played a critical role in cell toxicity induced by Al_2O_3 NPs, especially at the low exposure level (100 μg/ml Al_2O_3 NPs). However, the cell cycle arrest in A549 induced by high level Al_2O_3 NPs exposure (500μg/ml) was

mainly attributed to the interaction of modulated genes. Hereby, the functions of other cell cycle involved genes, which are showed in Table S5, still should be considered.

DNA damages were intensively reported to be associated with both cell death and cell cycle arrest. In the present study, a total of 28 genes associated with DNA damages were significantly modulated, which is predicted through GO enrichment analysis according to microarray data (Table S9). Among these genes, *BAX*, *BRCA1* are involved in both cell cycle and cell death; *TLK1*, *CLSPN*, *RAD17*, *BLM*, *APC*, *PTPRK* are involved in cell cycle; *BTG2*, *AEN*, *ADM*, *NUPR1* and *HIPK1* are involved in cell death. Enhanced expressions of *BAX*, *BRCA1*, *BLM*, *APC*, *PTPRK*, *AEN* and *NUPR1* were validated through qRT-PCR. Among these genes, overexpression of *BAX* was intensively reported to induce cell death and cell cycle arrest in A549 cells (de Souza et al., 2014, Xie and Yang, 2014, You and Park, 2014). *BRCA1* and *BLM* encode Fanconi anemia pathway proteins, which play a role in repair of inter-strand cross links. These two genes were reported to be up-regulated during S phage (Mjelle et al., 2015). AEN encodes apoptosis enhancing nuclease and promotes cell death via enhanced apoptosis.(Gato et al., 2014) *NUPR1*, also known as *p8* or *COM1*, is required for the expression genes involved in DNA repair, cell cycle regulation and apoptosis. In pancreatic cancer cells, upregulated *NUPR1* leads to stimulation of autophagy-mediated cell death (Hamidi et al., 2013). Therefore, our results strongly implicate that increased DNA damage could account for the enhanced cell death and cell cycle arrest.

Based on the genetic-associated disease model analysis, cancer and immune disorders were predicted based on the confirmed genes. These results showed associations between the

modulated gene expressions induced by exposure to Al_2O_3 NPs and the potential diseases, which suggests prospects for further studies.

Conclusions

Overall, a systematic biological approach based on Gene Ontology enrichment coupled with network analysis is presented hereby. It was used to reveal the key pathways involved in cellular responses to engineered Al_2O_3 NPs. Notably, it is hereby shown that Al_2O_3 NPs induced specific changes in gene expressions, with a pronounced up-regulation of genes related to the cell cycle and cell death, and indicate genes specifically associated with Al_2O_3 NPs. Further cell-based assays showed cell cycle arrest and cell death in A549s exposed to Al_2O_3 NPs, as well as the protective effects of *PTPN6* rescue, therefore corroborating the system-biology-based predictions. It is here proposed that an "omics" approach is used to identify perturbations in cellular functions in response to nano-scaled alumina material, which may help identify novel end-points of toxicity and increase comprehensive knowledge of potential toxicity. These results also reinforce the importance of validation through cell- or animal-based assays.

Declaration of interest

The authors declare no conflicts of interests. This work was financially supported by National Natural Science Foundation of China (Grant No. 81472938), the Fund of the Distinguished Talents of Jiangsu Province (BK20150021), the Natural Science Foundation of Jiangsu Province (BK20151418), the fund of the Distinguished Professor of Jiangsu Province, the Open Research Fund of State Key Laboratory of Bioelectronics , Southeast University and

the Fundamental Research Funds for the Central Universities. We thank Nanjing Milestone Biotechnology Co. LTD for the analysis of mRNA microarray profile.

REFERENCES

Adamcakova-Dodd A, Stebounova LV, O'Shaughnessy PT, Kim JS, Grassian VH,Thorne PS. 2012. Murine pulmonary responses after sub-chronic exposure to aluminum oxide-based nanowhiskers. Part Fibre Toxicol 9:22.

Alshatwi AA, Subbarayan PV, Ramesh E, Al-Hazzani AA, Alsaif MA,Alwarthan AA. 2013. Aluminium oxide nanoparticles induce mitochondrial-mediated oxidative stress and alter the expression of antioxidant enzymes in human mesenchymal stem cells. Food Addit Contam Part A Chem Anal Control Expo Risk Assess 30:1-10.

Bell ML, Belanger K, Ebisu K, Gent JF, Lee HJ, Koutrakis P,Leaderer BP. 2010. Prenatal exposure to fine particulate matter and birth weight: variations by particulate constituents and sources. Epidemiology 21:884-91.

Blomme EA, Yang Y,Waring JF. 2009. Use of toxicogenomics to understand mechanisms of drug-induced hepatotoxicity during drug discovery and development. Toxicol Lett 186:22-31.

Boverhof DR,Zacharewski TR. 2006. Toxicogenomics in risk assessment: applications and needs. Toxicol Sci 89:352-60.

Calero M, Gomez-Ramos A, Calero O, Soriano E, Avila J,Medina M. 2015. Additional mechanisms conferring genetic susceptibility to Alzheimer's disease. Front Cell Neurosci 9:138.

Cao R, Ding Q, Li P, Xue J, Zou Z, Huang J,Peng G. 2013. SHP1-mediated cell cycle redistribution inhibits radiosensitivity of non-small cell lung cancer. Radiat Oncol 8:178.

Cho J, Joshi MS,Sun CT. 2006. Effect of inclusion size on mechanical properties of polymeric composites with micro and nano particles. Composites Science and Technology 66:1941-52.

Cui Y,Paules RS. 2010. Use of transcriptomics in understanding mechanisms of drug-induced toxicity. Pharmacogenomics 11:573-85.

de Souza LR, Muehlmann LA, Dos Santos MS, Ganassin R, Simon-Vazquez R, Joanitti GA, Mosiniewicz-Szablewska E, Suchocki P, Morais PC, Gonzalez-Fernandez A, Azevedo RB,Bao SN. 2014. PVM/MA-shelled selol nanocapsules promote cell cycle arrest in A549 lung adenocarcinoma cells. J Nanobiotechnology 12:32.

Di Virgilio AL, Reigosa M, Arnal PM,Fernandez Lorenzo de Mele M. 2010. Comparative study of the cytotoxic and genotoxic effects of titanium oxide and aluminium oxide nanoparticles in Chinese hamster ovary (CHO-K1) cells. J Hazard Mater 177:711-8.

Dong Q, Siminovitch KA, Fialkow L, Fukushima T,Downey GP. 1999. Negative regulation of myeloid cell proliferation and function by the SH2 domain-containing tyrosine phosphatase-1. J Immunol 162:3220-30.

Ebisu K,Bell ML. 2012. Airborne PM2.5 chemical components and low birth weight in the northeastern and mid-Atlantic regions of the United States. Environ Health Perspect 120:1746-52.

Eom HJ, Chatterjee N, Lee J,Choi J. 2014. Integrated mRNA and micro RNA profiling reveals epigenetic mechanism of differential sensitivity of Jurkat T cells to AgNPs and Ag ions. Toxicol Lett 229:311-8.

Feliu N, Kohonen P, Ji J, Zhang Y, Karlsson HL, Palmberg L, Nystrom A,Fadeel B. 2015. Next-generation sequencing reveals low-dose effects of cationic dendrimers in primary human bronchial epithelial cells. ACS Nano 9:146-63.

Foldbjerg R, Irving ES, Hayashi Y, Sutherland DS, Thorsen K, Autrup H,Beer C. 2012. Global gene expression

profiling of human lung epithelial cells after exposure to nanosilver. Toxicol Sci 130:145-57.
Gato WE, McGee SR, Hales DB,Means JC. 2014. Time-Dependent Regulation of Apoptosis by AEN and BAX in Response to 2-Aminoanthracene Dietary Consumption. Toxicol Int 21:57-64.
Gerstein MB, Kundaje A, Hariharan M, Landt SG, Yan KK, Cheng C, Mu XJ, Khurana E, Rozowsky J, Alexander R, Min R, Alves P, Abyzov A, Addleman N, Bhardwaj N, Boyle AP, Cayting P, Charos A, Chen DZ, Cheng Y, Clarke D, Eastman C, Euskirchen G, Frietze S, Fu Y, Gertz J, Grubert F, Harmanci A, Jain P, Kasowski M, Lacroute P, Leng J, Lian J, Monahan H, O'Geen H, Ouyang Z, Partridge EC, Patacsil D, Pauli F, Raha D, Ramirez L, Reddy TE, Reed B, Shi M, Slifer T, Wang J, Wu L, Yang X, Yip KY, Zilberman-Schapira G, Batzoglou S, Sidow A, Farnham PJ, Myers RM, Weissman SM,Snyder M. 2012. Architecture of the human regulatory network derived from ENCODE data. Nature 489:91-100.
Gurunathan S, Jeong JK, Han JW, Zhang XF, Park JH,Kim JH. 2015. Multidimensional effects of biologically synthesized silver nanoparticles in Helicobacter pylori, Helicobacter felis, and human lung (L132) and lung carcinoma A549 cells. Nanoscale Res Lett 10:35.
Hamidi T, Cano CE, Grasso D, Garcia MN, Sandi MJ, Calvo EL, Dagorn JC, Lomberk G, Goruppi S, Urrutia R, Carracedo A, Velasco G,Iovanna JL. 2013. NUPR1 works against the metabolic stress-induced autophagy-associated cell death in pancreatic cancer cells. Autophagy 9:95-7.
Hanagata N, Zhuang F, Connolly S, Li J, Ogawa N,Xu M. 2011. Molecular responses of human lung epithelial cells to the toxicity of copper oxide nanoparticles inferred from whole genome expression analysis. ACS Nano 5:9326-38.
Hussain SM, Hess KL, Gearhart JM, Geiss KT,Schlager JJ. 2005. In vitro toxicity of nanoparticles in BRL 3A rat liver cells. Toxicol In Vitro 19:975-83.
Ingvarsson PT, Rasmussen IS, Viaene M, Irlik PJ, Nielsen HM,Foged C. 2014. The surface charge of liposomal adjuvants is decisive for their interactions with the Calu-3 and A549 airway epithelial cell culture models. Eur J Pharm Biopharm 87:480-8.
Khalil AM, Cambier JC,Shlomchik MJ. 2012. B cell receptor signal transduction in the GC is short-circuited by high phosphatase activity. Science 336:1178-81.
Lai X, Wei Y, Zhao H, Chen S, Bu X, Lu F, Qu D, Yao L, Zheng J,Zhang J. 2015. The effect of Fe2 O3 and ZnO nanoparticles on cytotoxicity and glucose metabolism in lung epithelial cells. J Appl Toxicol 35:651-64.
Lee JH, Chiang SY, Nam D, Chung WS, Lee J, Na YS, Sethi G,Ahn KS. 2014. Capillarisin inhibits constitutive and inducible STAT3 activation through induction of SHP-1 and SHP-2 tyrosine phosphatases. Cancer Lett 345:140-8.
Li XB, Zheng H, Zhang ZR, Li M, Huang ZY, Schluesener HJ, Li YY,Xu SQ. 2009. Glia activation induced by peripheral administration of aluminum oxide nanoparticles in rat brains. Nanomedicine 5:473-9.
Lopez-Ruiz P, Rodriguez-Ubreva J, Cariaga AE, Cortes MA,Colas B. 2011. SHP-1 in cell-cycle regulation. Anticancer Agents Med Chem 11:89-98.
Lu S, Zhang W, Zhang R, Liu P, Wang Q, Shang Y, Wu M, Donaldson K,Wang Q. 2015. Comparison of cellular toxicity caused by ambient ultrafine particles and engineered metal oxide nanoparticles. Part Fibre Toxicol 12:5.
Mascelloni M, Delgado-Saborit JM, Hodges NJ,Harrison RM. 2015. Study of gaseous benzene effects upon A549 lung epithelial cells using a novel exposure system. Toxicol Lett 237:38-45.
Mittal S,Pandey AK. 2014. Cerium oxide nanoparticles induced toxicity in human lung cells: role of ROS mediated DNA damage and apoptosis. Biomed Res Int 2014:891934.
Mjelle R, Hegre SA, Aas PA, Slupphaug G, Drablos F, Saetrom P,Krokan HE. 2015. Cell cycle regulation of human DNA repair and chromatin remodeling genes. DNA Repair (Amst) 30:53-67.

Murayama KS, Kametani F, Saito S, Kume H, Akiyama H,Araki W. 2006. Reticulons RTN3 and RTN4-B/C interact with BACE1 and inhibit its ability to produce amyloid beta-protein. Eur J Neurosci 24:1237-44.
Nymark P, Wijshoff P, Cavill R, van Herwijnen M, Coonen ML, Claessen S, Catalan J, Norppa H, Kleinjans JC,Briede JJ. 2015. Extensive temporal transcriptome and microRNA analyses identify molecular mechanisms underlying mitochondrial dysfunction induced by multi-walled carbon nanotubes in human lung cells. Nanotoxicology 1-12.
Oberdorster G, Oberdorster E,Oberdorster J. 2005. Nanotoxicology: an emerging discipline evolving from studies of ultrafine particles. Environ Health Perspect 113:823-39.
Oertle T, Huber C, van der Putten H,Schwab ME. 2003. Genomic structure and functional characterisation of the promoters of human and mouse nogo/rtn4. J Mol Biol 325:299-323.
Pathak AK, Bhutani M, Nair AS, Ahn KS, Chakraborty A, Kadara H, Guha S, Sethi G,Aggarwal BB. 2007. Ursolic acid inhibits STAT3 activation pathway leading to suppression of proliferation and chemosensitization of human multiple myeloma cells. Mol Cancer Res 5:943-55.
Popat KC, Mor G, Grimes CA,Desai TA. 2004. Surface modification of nanoporous alumina surfaces with poly(ethylene glycol). Langmuir 20:8035-41.
Prabhakar PV, Reddy UA, Singh SP, Balasubramanyam A, Rahman MF, Indu Kumari S, Agawane SB, Murty US, Grover P,Mahboob M. 2012. Oxidative stress induced by aluminum oxide nanomaterials after acute oral treatment in Wistar rats. J Appl Toxicol 32:436-45.
Reff A, Bhave PV, Simon H, Pace TG, Pouliot GA, Mobley JD,Houyoux M. 2009. Emissions inventory of PM2.5 trace elements across the United States. Environ Sci Technol 43:5790-6.
Rodriguez-Ubreva FJ, Cariaga-Martinez AE, Cortes MA, Romero-De Pablos M, Ropero S, Lopez-Ruiz P,Colas B. 2010. Knockdown of protein tyrosine phosphatase SHP-1 inhibits G1/S progression in prostate cancer cells through the regulation of components of the cell-cycle machinery. Oncogene 29:345-55.
Shim W, Paik MJ, Nguyen DT, Lee JK, Lee Y, Kim JH, Shin EH, Kang JS, Jung HS, Choi S, Park S, Shim JS,Lee G. 2012. Analysis of changes in gene expression and metabolic profiles induced by silica-coated magnetic nanoparticles. ACS Nano 6:7665-80.
Shrivastava R, Raza S, Yadav A, Kushwaha P,Flora SJ. 2014. Effects of sub-acute exposure to TiO2, ZnO and Al2O3 nanoparticles on oxidative stress and histological changes in mouse liver and brain. Drug Chem Toxicol 37:336-47.
Simon-Deckers A, Gouget B, Mayne-L'hermite M, Herlin-Boime N, Reynaud C,Carriere M. 2008. In vitro investigation of oxide nanoparticle and carbon nanotube toxicity and intracellular accumulation in A549 human pneumocytes. Toxicology 253:137-46.
Sooman L, Ekman S, Tsakonas G, Jaiswal A, Navani S, Edqvist PH, Ponten F, Bergstrom S, Johansson M, Wu X, Blomquist E, Bergqvist M, Gullbo J,Lennartsson J. 2014. PTPN6 expression is epigenetically regulated and influences survival and response to chemotherapy in high-grade gliomas. Tumour Biol 35:4479-88.
Srikanth K, Mahajan A, Pereira E, Duarte AC,Venkateswara Rao J. 2015. Aluminium oxide nanoparticles induced morphological changes, cytotoxicity and oxidative stress in Chinook salmon (CHSE-214) cells. J Appl Toxicol
Sun Z, Pan X, Zou Z, Ding Q, Wu G,Peng G. 2015. Increased SHP-1 expression results in radioresistance, inhibition of cellular senescence, and cell cycle redistribution in nasopharyngeal carcinoma cells. Radiat Oncol 10:152.
Teng FY,Tang BL. 2013. Nogo/RTN4 isoforms and RTN3 expression protect SH-SY5Y cells against multiple death insults. Mol Cell Biochem 384:7-19.
Thenmozhi AJ, Raja TR, Janakiraman U,Manivasagam T. 2015. Neuroprotective effect of hesperidin on

aluminium chloride induced Alzheimer's disease in Wistar rats. Neurochem Res 40:767-76.
Tuomela S, Autio R, Buerki-Thurnherr T, Arslan O, Kunzmann A, Andersson-Willman B, Wick P, Mathur S, Scheynius A, Krug HF, Fadeel B,Lahesmaa R. 2013. Gene expression profiling of immune-competent human cells exposed to engineered zinc oxide or titanium dioxide nanoparticles. PLoS One 8:e68415.
Veranth JM, Kaser EG, Veranth MM, Koch M,Yost GS. 2007. Cytokine responses of human lung cells (BEAS-2B) treated with micron-sized and nanoparticles of metal oxides compared to soil dusts. Part Fibre Toxicol 4:2.
Wagner AJ, Bleckmann CA, Murdock RC, Schrand AM, Schlager JJ,Hussain SM. 2007. Cellular interaction of different forms of aluminum nanoparticles in rat alveolar macrophages. J Phys Chem B 111:7353-9.
Wang Z, Gerstein M,Snyder M. 2009. RNA-Seq: a revolutionary tool for transcriptomics. Nat Rev Genet 10:57-63.
Witzig TE, Hu G, Offer SM, Wellik LE, Han JJ, Stenson MJ, Dogan A, Diasio RB,Gupta M. 2014. Epigenetic mechanisms of protein tyrosine phosphatase 6 suppression in diffuse large B-cell lymphoma: implications for epigenetic therapy. Leukemia 28:147-54.
Xie QC,Yang YP. 2014. Anti-proliferative of physcion 8-O-beta-glucopyranoside isolated from Rumex japonicus Houtt. on A549 cell lines via inducing apoptosis and cell cycle arrest. BMC Complement Altern Med 14:377.
You BR,Park WH. 2014. Zebularine inhibits the growth of A549 lung cancer cells via cell cycle arrest and apoptosis. Mol Carcinog 53:847-57.
Zhang QL, Jia L, Jiao X, Guo WL, Ji JW, Yang HL,Niu Q. 2012. APP/PS1 transgenic mice treated with aluminum: an update of Alzheimer's disease model. Int J Immunopathol Pharmacol 25:49-58.
Zhang W, Shi Y, Chen Y, Yu S, Hao J, Luo J, Sha X,Fang X. 2010. Enhanced antitumor efficacy by paclitaxel-loaded pluronic P123/F127 mixed micelles against non-small cell lung cancer based on passive tumor targeting and modulation of drug resistance. Eur J Pharm Biopharm 75:341-53.

Supporting information

Supplementary information available online, Figure S1-S5, Table S1-S9.

Figure legends

Figure 1. The Gene Ontology enrichment identified by the hypergeometric test on annotations and pathway analysis of cell death and cell cycle involved genes.

A: the sub-ontology biological process (BP) shows that cell cycle encompassing 41/302 genes and cell death encompassing 35/302 genes are the mostly involved enrichment categories. B: gene-transcription factors network analysis shows that *PTPN6*, *IER3* and *RTN4* play central roles in this regulatory network.

Figure 2. qRT-PCR results of the expression level of modulated mRNA with cut-off as fold change >2.0.

A:Gene expression level in Al_2O_3 NPs treated A549 cells. *CPNE7*, *ATP6UOD2,* N*EMF, CD44*, *SQSTM1*, *HSPA6*, *ZBTB7C*, *SLTM*, and *SRPK2* were upregulated, RPL37 and CCDC68 were downregulated by Al_2O_3 NPs in a dose-dependent manner. B: Gene expression level in Al_2O_3 NPs exposed mice lung tissues. Except that HSPA6 is not expressed in mice, the other ten genes showed the same trend in regulation with cell-based assay C: Except *CCDC68,* the fold changes of modulated genes in 100 μg/ml Al_2O_3 NPs treated A549 cellswere consistent with array data.

Figure 3. Expression levels ofcell cycle and cell death involved genes.

A: A total of 22/30 cell cycle-related gene expressions were confirmed in A549 cells. B: The same 22 cell cycle-related gene expressions were confrimed in mice lung tissues. C: A total of 22/30 cell death-related gene expressions were validated in A549 cells. D: The same 22 cell death-related gene expressions were validated in mice lung tissues.

Figure 4. Cell viability and cell cycle arrest of A549 cells after exposure to Al_2O_3 NPs.

A: cell viability of A549 cells after exposure to Al_2O_3 NPs. Cell toxicity was evident in the 25, 50, 100, 250, 500 and 1 000 μg/ml Al_2O_3 NPs groups 24 h after treatment. B: Flow cytometric analysis demonstrated cell death induced by Al_2O_3 NPs exposure. C: G2/S phase cell cycle arrest induced by Al_2O_3 NPs exposure.

Figure 5. Bioinformatic analyses based on the confirmed cell cycle and cell death related genes.

A: The top 10 Gene Ontology enrichment categories showed that the mitosis related GO categories are most strongly enriched. B: Gene-transcription factor network analysis based on the confirmed genes, *PTPN6, BAX, IER3* and *RTN4* play roles in this network. C: The key transcription factors and mRNA regulated by *PTPN6* and the heatmap of *PTPN6, APP, BAX, PDCD4*.

Figure 6. The protective effects of PTPN6 rescue.

A: Expression level of PTPN6 were increased after plasmid transfection. B: Overexpression of PTPN6 prevented Al_2O_3 NPs induced A549 cell death. C: PTPN6 rescue partially restore the normal cell cycle of A549 cells.

Figure 1

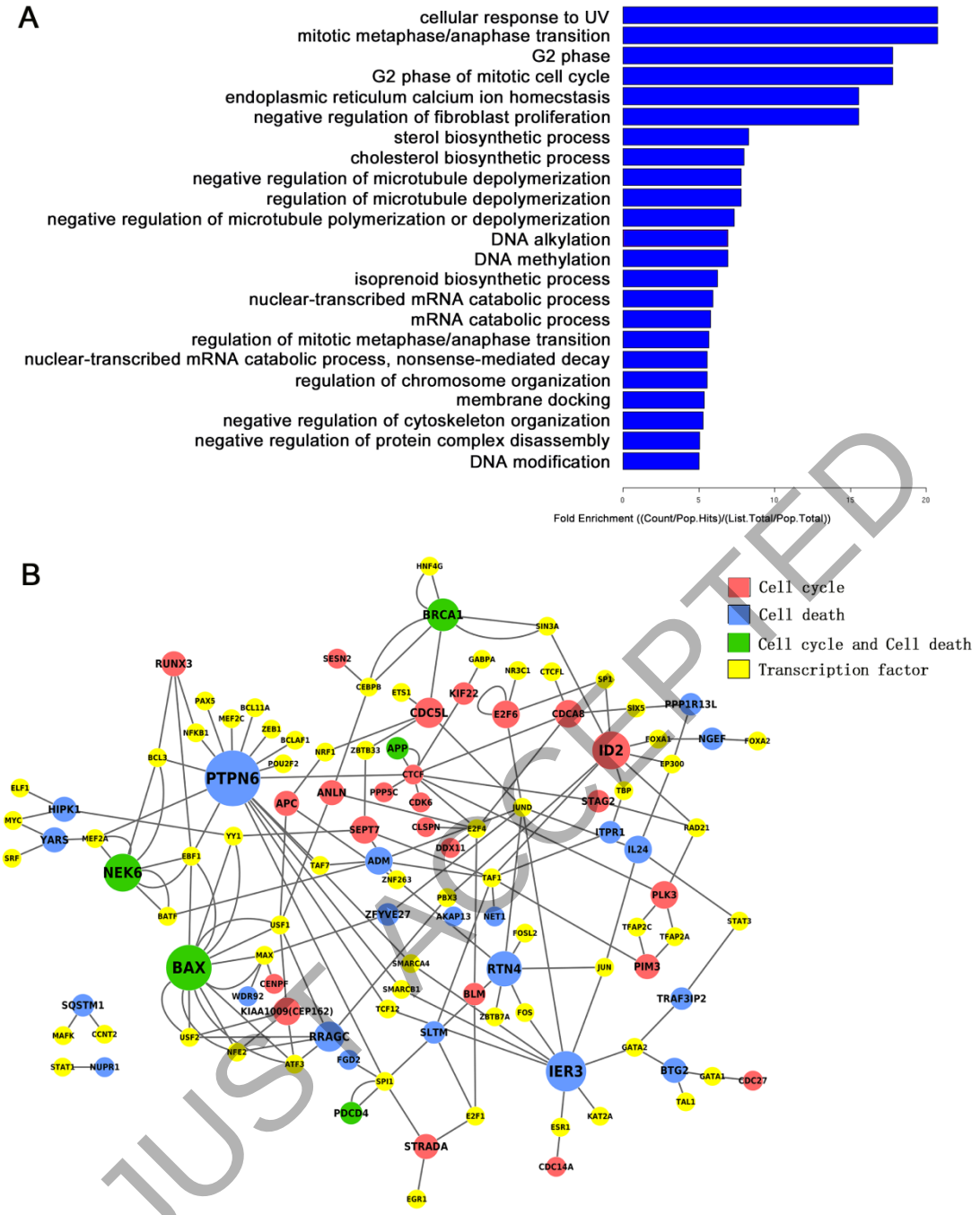

Figure 2

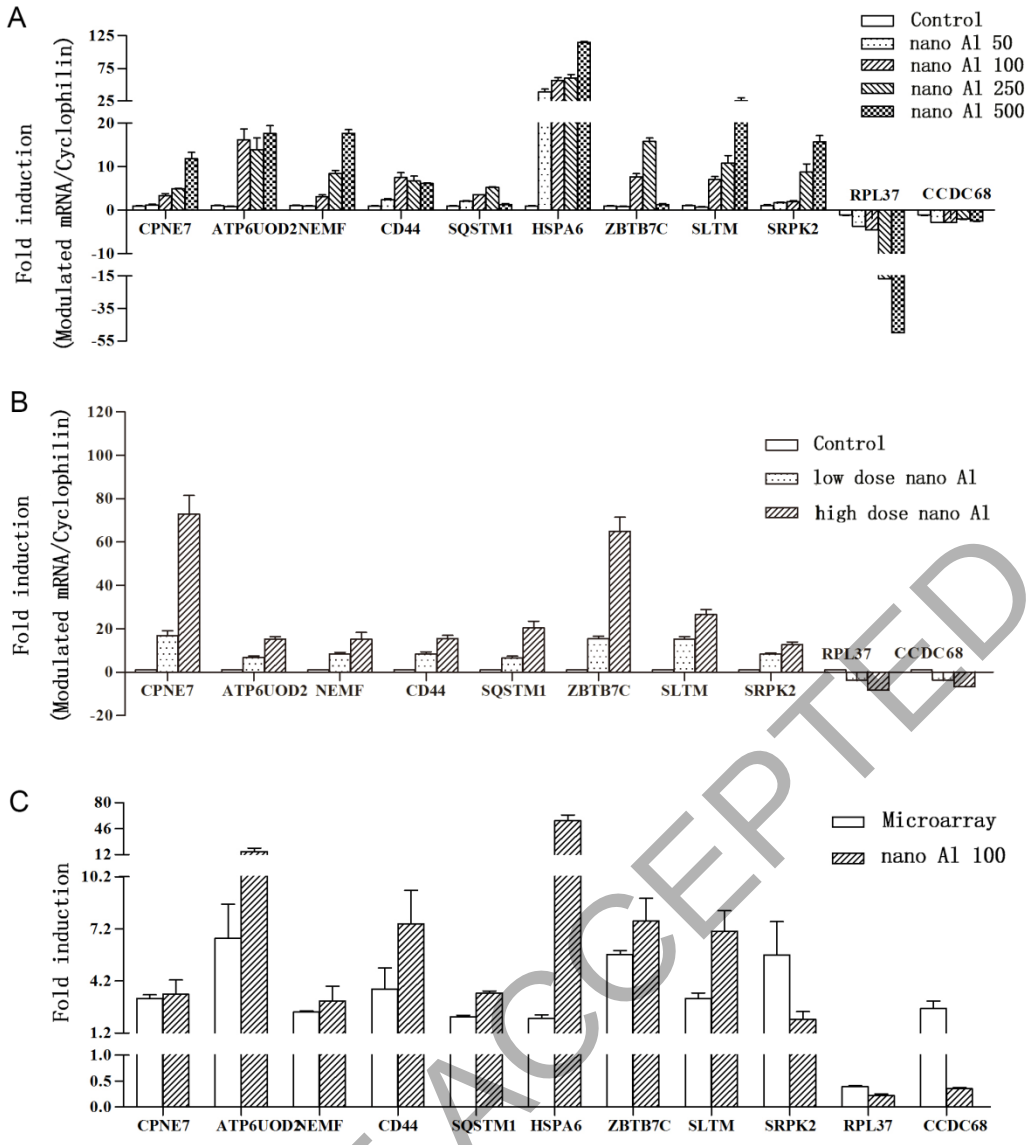

Figure 3

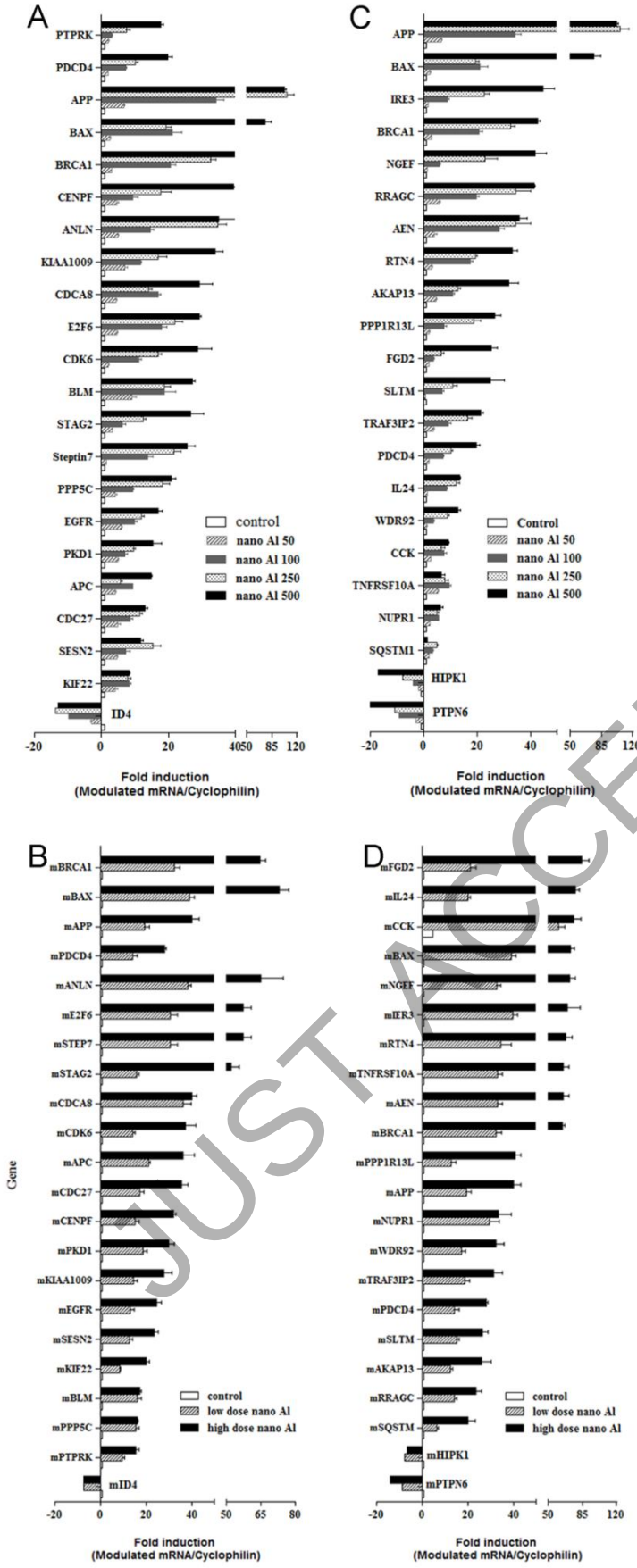

Figure 4

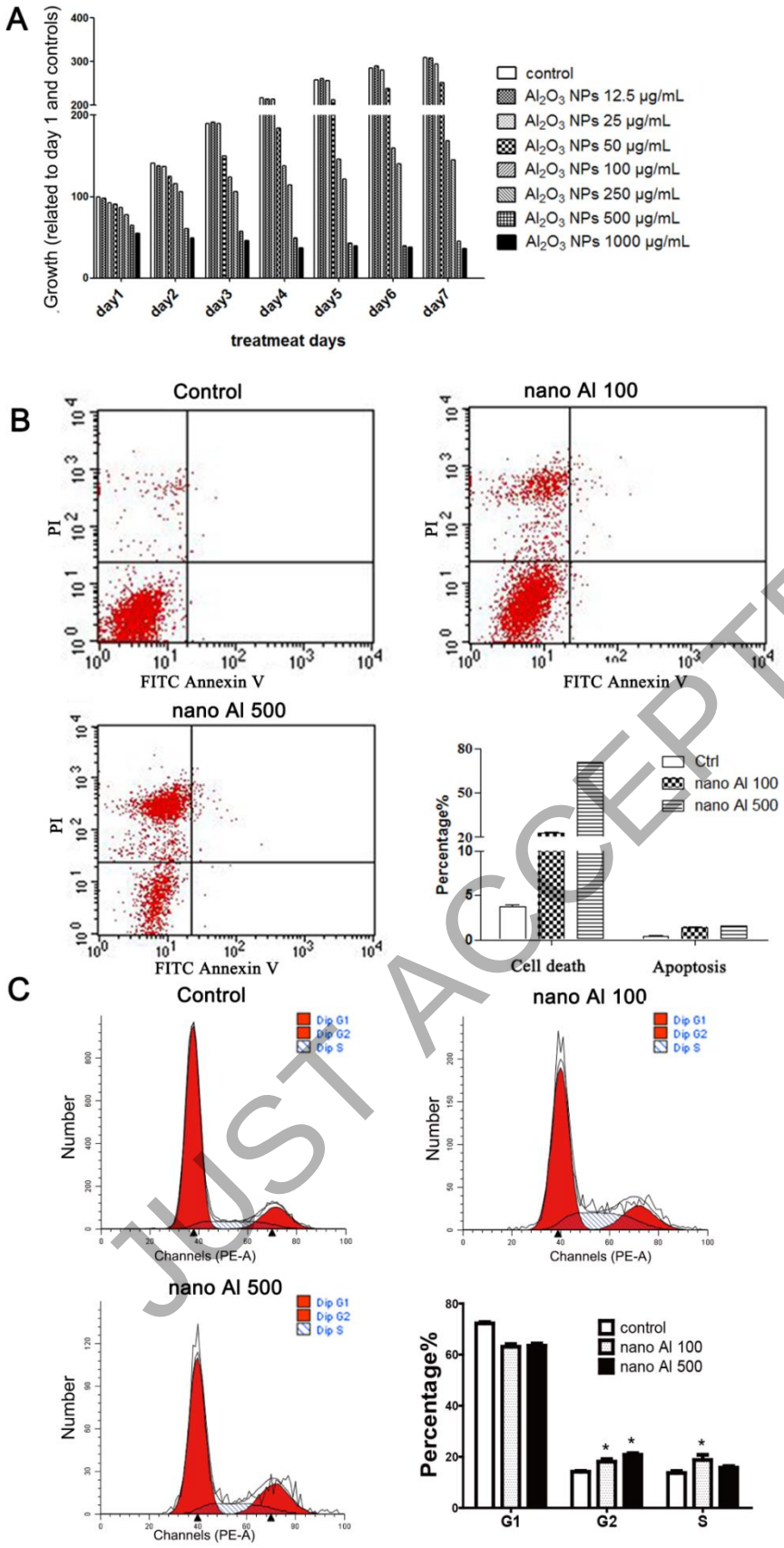

Figure 5

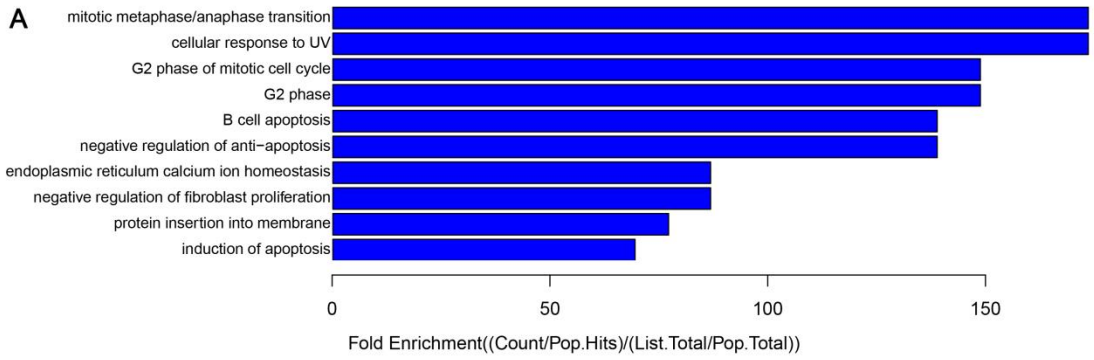

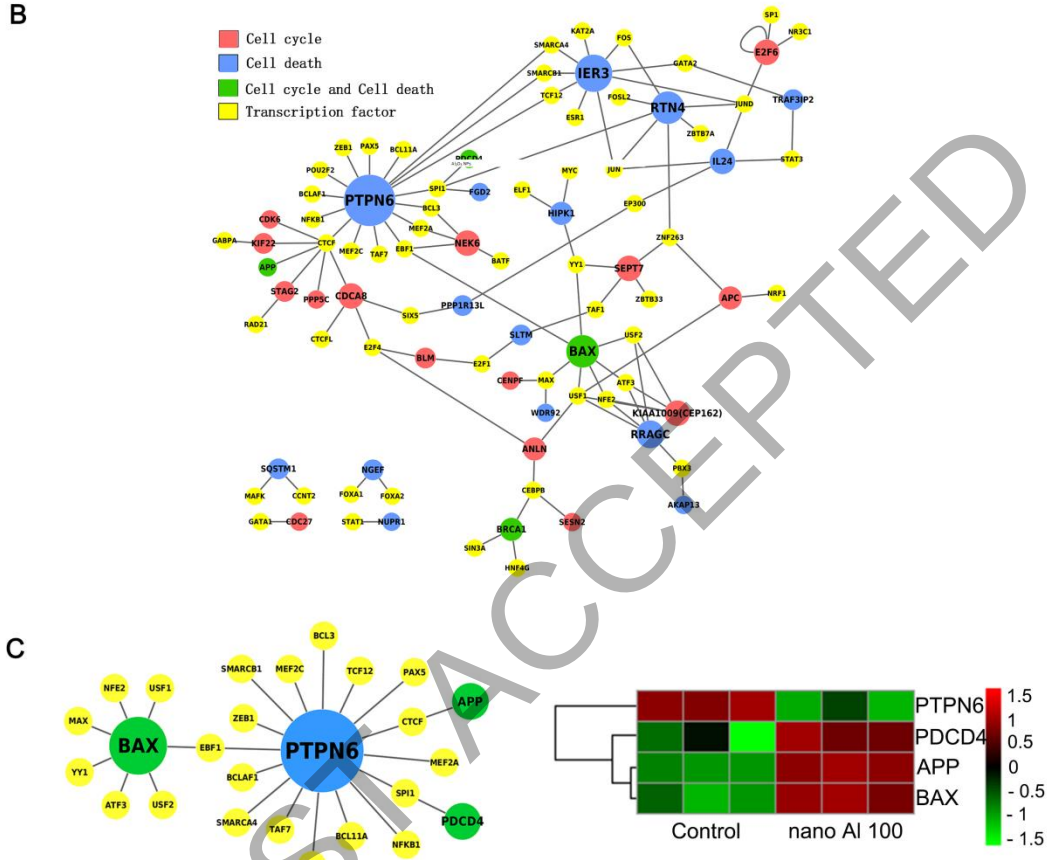

Figure 6